International Journal of Plasticity, Vol. 8, pp. 425-452, 1992
Printed in the U.S.A.

0749-6419/92 \$5.00 + .00

ANALYSIS OF SHEAR BANDING IN TWELVE MATERIALS

R. C. BATRA and C. H. KIM

University of Missouri-Rolla

Abstract—The problem of the initiation and growth of shear bands in 12 different materials, namely, OFHC copper, Cartridge brass, Nickel 200, Armco IF (interstitial free) iron, Carpenter electric iron, 1006 steel, 2024-T351 aluminum, 7039 aluminum, low alloy steel, S-7 tool steel, Tungsten alloy, and Depleted Uranium (DU −0.75 Ti) is studied with the objectives of finding out when a shear band initiates, and upon what parameters does the band width depend. The nonlinear coupled partial differential equations governing the overall simple shearing deformations of a thermally softening viscoplastic block are analyzed. It is assumed that the thermomechanical response of these materials can be adequately represented by the Johnson-Cook law, and the only inhomogeneity present in the block is the variation in its thickness. The effect of the defect size on the initiation and subsequent growth of the band is also studied. It is found that, for each one of these 12 materials, the deformation has become nonhomogeneous by the time the maximum shear stress occurs. Also the band width, computed when the shear stress has dropped to 85% of its peak value, does not correlate well with the thermal conductivity of the material. The band begins to grow rapidly when the shear stress has dropped to 90% of its maximum value.

I. INTRODUCTION

JOHNSON [1987] has pointed out that TRESCA [1878] was the first to observe hot lines during the forging of a platinum bar. TRESCA stated that these were the lines of greatest development of heat. Subsequently, MASSEY [1921] observed these hot lines during the hot forging of a metal, and stated that "when diagonal 'slipping' takes place, there is great friction between particles and a considerable amount of heat is generated." These hot lines are now referred to as shear bands. Their study is attracting considerable attention because shear bands usually precede shear fractures, and once a shear band has formed, subsequent deformations of the body occur in this narrow region, and the strength of the rest of the body is not fully utilized.

The experimental observations of the shear banding phenomenon in metals deformed at high strain rates reported by ZENER and HOLLOMON [1944], MOSS [1981], COSTIN *et al.* [1979], HARTLEY *et al.* [1987], WULF [1978], and MARCHAND and DUFFY [1988] have contributed to our understanding of the initiation and growth of shear bands. The analytical works (RECHT [1964], STAKER [1981], CLIFTON [1980], MOLINARI and CLIFTON [1987], BURNS [1985], and WRIGHT [1990]) and numerical works (MERZER [1982], WRIGHT and BATRA [1985], WRIGHT and WALTER [1987], BATRA [1987], SHAWKI and CLIFTON [1989], and BATRA and KIM [1990]) aimed at understanding factors that enhance or inhibit the initiation and subsequent development of shear bands have involved analyzing overall simple shearing deformations of a viscoplastic block. SHAWKI and CLIFTON [1989] have reviewed much of the literature on shear banding. Recently, LEMONDS and NEEDLEMAN [1986a, 1986b], NEEDLEMAN [1989], BATRA and LIU [1989, 1990], ANAND *et al.* [1988], and ZHU and BATRA [1990] have studied the phenomenon of shear banding in plane strain deformations of a viscoplastic solid.

Here we study the response of six ductile and six less ductile (the last six materials listed in the abstract) materials subjected to the same hypothetical simple shearing test at a nominal strain-rate of 1,500 $\sec^{-1}$. Three of these ductile materials, OFHC copper, Cartridge brass, and Nickel 200, are fcc, and the other three ductile materials, Armco IF (interstitial free) iron, Carpenter electrical iron, and 1006 steel, are bcc iron base alloys. Each of these 12 materials is assumed to obey the JOHNSON–COOK [1983] law, and the material parameters are assigned values given by JOHNSON *et al.* [1983]. The computed results reveal that the localization of the deformation begins earnestly when the shear stress at the weakest point in the specimen has dropped to somewhere between 90 and 95% of its maximum value. The ratio of the maximum shear strain within the band to the nominal strain is found to depend strongly upon log δ, where δ is the percentage decrease in the specimen thickness at the center as compared to that at its edges. Larger defects result in more severe localization of the deformation for the same value of the ratio of the shear stress to the maximum shear stress.

II. FORMULATION OF THE PROBLEM

Equations governing the dynamic thermomechanical deformations of a viscoplastic block, shown in Fig. 1 and undergoing overall adiabatic simple shearing deformations, are

$$\rho w \dot{v} = (ws)_{,y}, \qquad 0 < y < H, \tag{1}$$

$$\rho w \dot{e} = -(wq)_{,y} + ws\dot{\gamma}, \quad 0 < y < H, \tag{2}$$

$$\dot{\gamma} = v_{,y}, \tag{3}$$

$$\dot{\gamma} = \dot{\gamma}_e + \dot{\gamma}_p, \tag{4}$$

$$q = -k\theta_{,y}, \tag{5}$$

$$\dot{s} = \mu\dot{\gamma}_e, \tag{6}$$

$$\rho\dot{e} = \rho c\dot{\theta} + s\dot{\gamma}_e, \tag{7}$$

$$\dot{\gamma}_p = \dot{\gamma}_0 \exp\left[\left(\frac{s}{(A + B\gamma_p^n)(1 - \theta/\theta_m)} - 1.0\right)\Big/ D\right]. \tag{8}$$

Here ρ is the mass density, v the velocity of a material particle in the direction of shearing, w the thickness of the block, s the shearing stress, θ the temperature rise, a comma followed by y signifies partial differentiation with respect to y, and a superimposed dot indicates the material time derivative. Furthermore, e is the specific internal energy, q the heat flux, γ the shearing strain, μ the shear modulus of the material of the block, k the thermal conductivity, and c equals its specific heat. Whereas eqns (1) and (2) express, respectively, the balance of linear momentum and the balance of internal energy, eqns (5) through (8) are constitutive hypotheses. Equation (5) is the familiar Fourier's law of heat conduction, eqn (6) Hooke's law written in the rate form, and eqn (8) is the Johnson–Cook law. In it, $\dot{\gamma}_0$ is the reference strain-rate, θ_m equals the melting temperature of the material, and parameters n and D characterize, respectively, the strain and

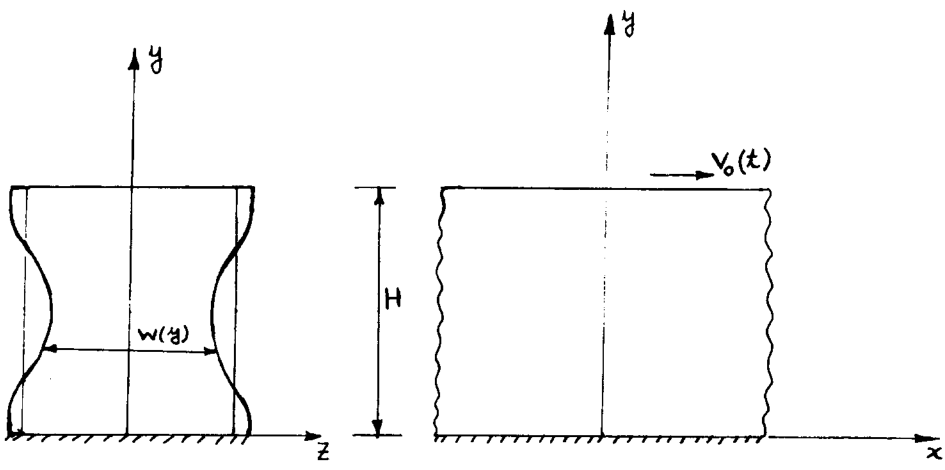

Fig. 1. Problem studied.

strain-rate hardening characteristics of the material. Material parameters ρ, k, μ, A, B, n, and D are presumed to be constants for the range of strains and temperatures for the problem. The main reason for modeling the material response by the Johnson–Cook law is the availability of the values of material parameters A, B, n, θ_m, and D for the 12 materials. We note that Johnson and Cook determined the values of these parameters from torsional test data over a limited range of strain rates and temperatures. The range of strain rates and temperatures anticipated to occur within a shear band is considerably more than that used to calibrate the flow rule (8). Also, for some materials, phase changes may occur within a band. Thus, the results presented herein are approximate, and help establish general trends.

Besides the choice of the appropriate constitutive relation alluded to above, one also needs to study a three-dimensional problem in order to capture all of the details of the deformation. The plot of the shear strain distribution at three separate locations on the circumference of the tubular specimen given in figure 6 of Marchand and Duffy's [1988] paper indicates that the problem is not even axisymmetric. However, an approximate solution of the three-dimensional problem requires computational resources unavailable to most university researchers. Equations (1) and (2) may be viewed as balance laws integrated over the thickness of the tubular specimen and implicitly assume that the inner and outer cylindrical surfaces of the tubular specimen are traction free, and the heat loss from these surfaces to the surroundings is negligible. We note that the tubular specimens are typically loaded at the ends, and the test is completed in microseconds, so that the heat dissipated from the cylindrical surfaces is indeed very small. Similar models have been used by Molinari and Clifton [1987], Wright [1990], and Shawki and Clifton [1989] to analyze the shear band problem.

Substitution for $\dot{e}$ from eqn (7) and for q from eqn (5) into eqn (2) gives

$$\rho w c \dot{\theta} = k(w\theta_{,y})_{,y} + ws\dot{\gamma}_p. \tag{9}$$

We have assumed here that all of the plastic working, given by the second term on the right-hand side of eqn (9), is converted into heat, whereas Sulijoadikusumo and Dil-

LON [1979] and FARREN and TAYLOR [1925] found that only 90 to 95% of the plastic work done is responsible for raising the temperature of the body.

In terms of nondimensional variables, indicated below by a superimposed bar,

$$
\begin{gathered}
\bar{y} = y/H, \quad \bar{w} = w/H, \quad \bar{t} = tv_0/H, \quad \bar{\theta} = \theta/\theta_0, \quad \theta_0 = \sigma_0/\rho c, \\
\bar{s} = s/\sigma_0, \quad \bar{A} = A/\sigma_0, \quad \bar{B} = B/\sigma_0, \quad \bar{\mu} = \mu/\sigma_0, \\
\alpha = \rho v_0^2/\sigma_0, \quad \beta = k/(\rho v_0 c H), \quad \dot{\bar{\gamma}} = \dot{\gamma} H/v_0,
\end{gathered}
\tag{10}
$$

eqns (1), (6), (8), and (9) become

$$\alpha w \dot{v} = (ws)_{,y}, \tag{11}$$

$$\dot{s} = \mu(v_{,y} - \dot{\gamma}_p), \tag{12}$$

$$\dot{\gamma}_p = \dot{\gamma}_0 \exp\left[\left(\frac{s}{(A + B\gamma_p^n)(1 - \theta/\theta_m)} - 1.0\right)/D\right], \tag{13}$$

$$w\dot{\theta} = \beta(w\theta_{,y})_{,y} + ws\dot{\gamma}_p \tag{14}$$

where we have dropped the superimposed bars. In eqns (10), v_0 is the final value of the speed imposed on the top surface of the block, and σ_0 is the yield stress in a quasistatic simple shearing test. We note that the value of α in eqn (11) signifies the effect of inertia forces compared to the flow stress of the material. For boundary conditions we take

$$
\begin{aligned}
\theta(0,t) &= 0, \quad \theta(1,t) = 0, \quad v(0,t) = 0, \\
v(1,t) &= t/0.01, \quad 0 \le t \le 0.01, \\
&= 1, \qquad t \ge 0.01
\end{aligned}
\tag{15}
$$

and for initial conditions,

$$v(y,0) = 0, \quad s(y,0) = 0, \quad \theta(y,0) = 0. \tag{16}$$

That is, the block is initially at rest, is stress free, and is at a uniform temperature. The lower and upper surfaces of the block are kept at a constant temperature by the loading devices (grips) which act as heat sinks, the lower surface is kept fixed while on the top surface, the prescribed shearing speed increases from 0 to 1.0 in a nondimensional time of 0.01. For the thickness variation we take

$$w(y) = w_0\left[1 + \frac{\delta}{2}\sin\left(\frac{1}{2} + 2y\right)\pi\right]. \tag{17}$$

That is, the block is thinnest at the center ($y = 1/2$) and thickest at the bounding surfaces ($y = 0,1$).

We note that the coupled partial differential eqns (11) through (14) are highly nonlinear. An approximate solution of these equations under the side conditions (15) and (16) with w given by (17) is sought by the finite element method. The governing equations are first reduced to a set of coupled ordinary differential equations by using the Galerkin approximation. These equations are then integrated with respect to time t by the GEAR [1971] method. For this purpose the subroutine LSODE included in the package ODEPACK developed by HINDMARSH [1983] is used. BATRA and KIM [1990] have given the details of the method.

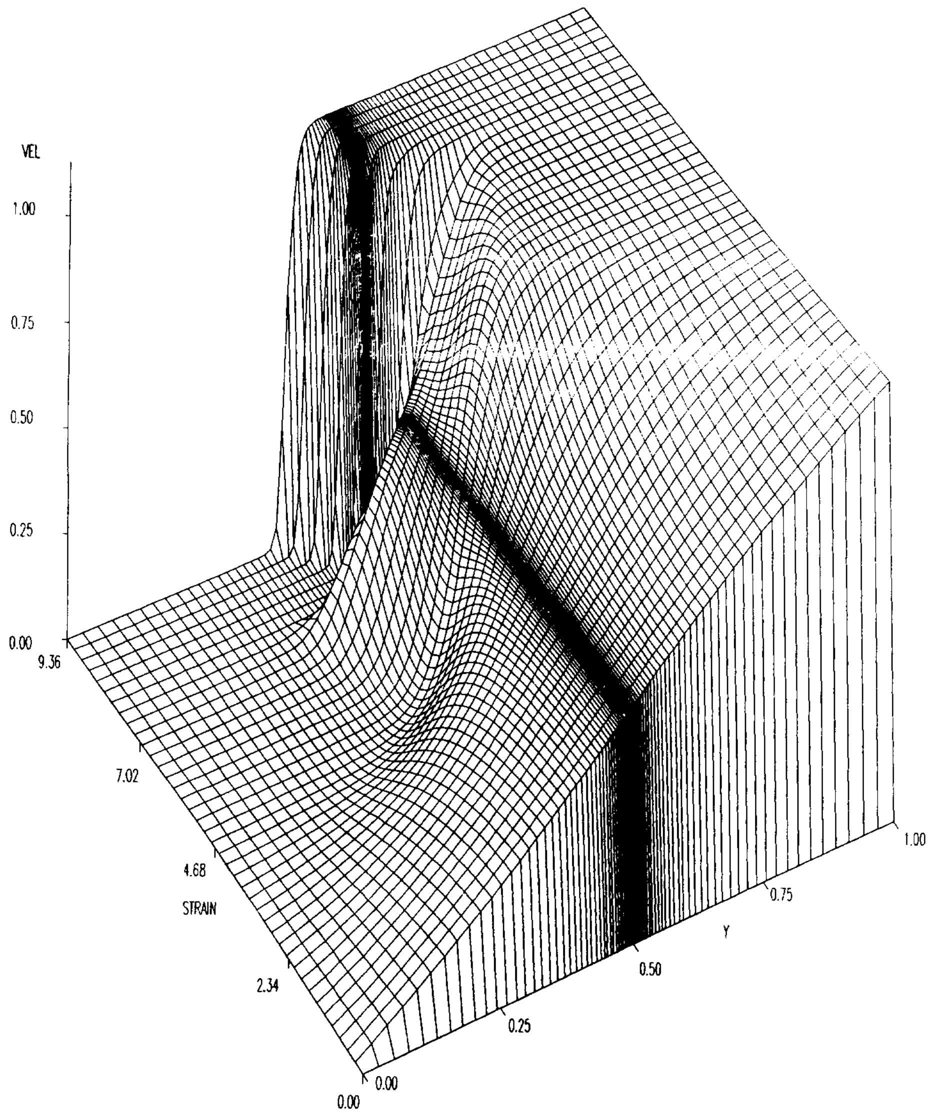

Fig. 2a. The evolution of the velocity field within the viscoplastic block being sheared at a nominal strain-rate of 1500 sec^{-1} for OFHC copper. (*Figure continued*)

III. DISCUSSION OF RESULTS

In order to compute results, we assigned the following values to variables that are common to all materials.

$$H = 3.18 \text{ mm}, \qquad v_0 = 4.77 \text{ m/sec}, \qquad w_0 = 0.248, \qquad \delta = 0.05. \tag{18}$$

Thus, the block is sheared at a nominal strain-rate of 1500 sec^{-1}, and its thickness at the center is 5% less than that at the outer edges. The finite element mesh used is such

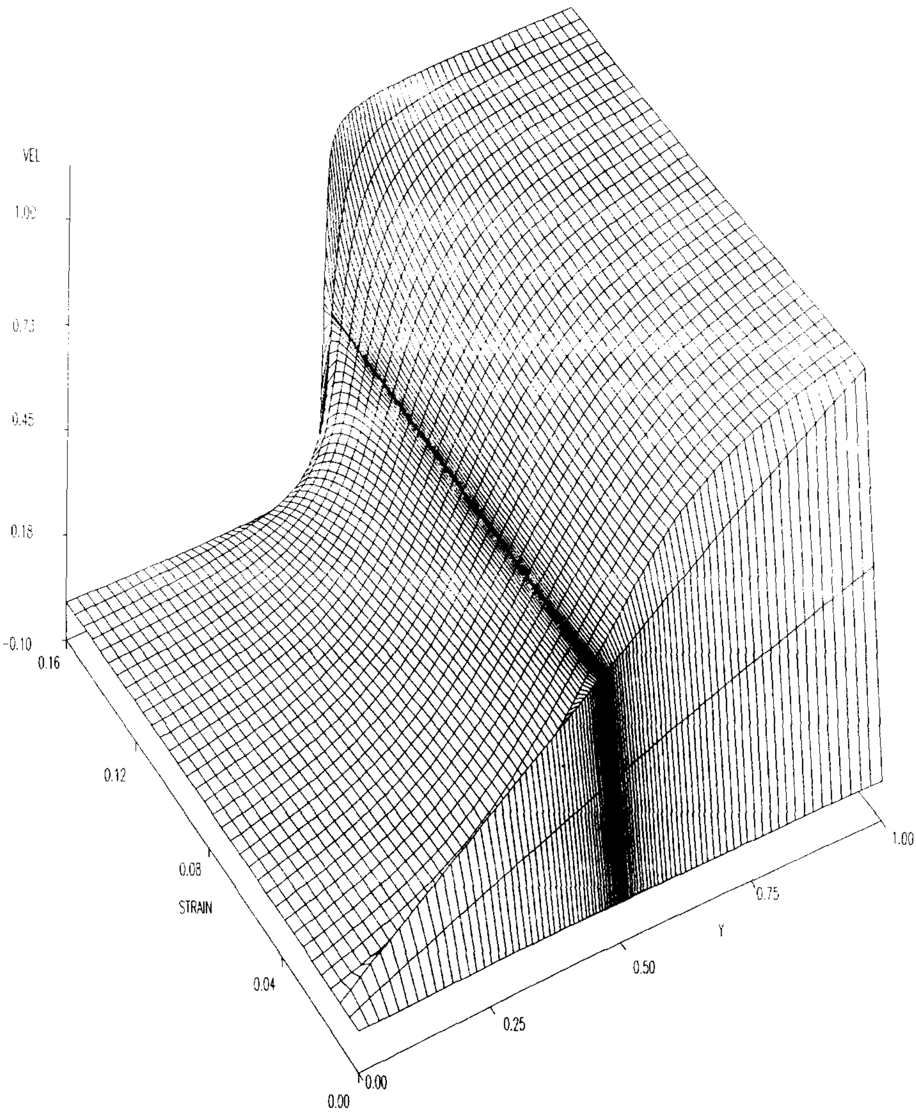

Fig. 2b. The evolution of the velocity field within the viscoplastic block being sheared at a nominal strain-rate of 1500 sec^{-1} for S-7 tool steel.

that a large number of nodes are concentrated near the center, where the shear band is expected to develop. The y-coordinate of the nth node is given by

$$y_n = 4\left[\frac{n-1}{100} - 0.5\right]^3 + \frac{1}{2}, \quad n = 1,2,3,\ldots,101.$$

Values of other parameters, taken either from the paper by Johnson *et al.* [1983] or from a handbook, are listed in Table 1. Also listed in the table are the computed values of the nondimensional mass density and the nondimensional thermal conductivity. As has

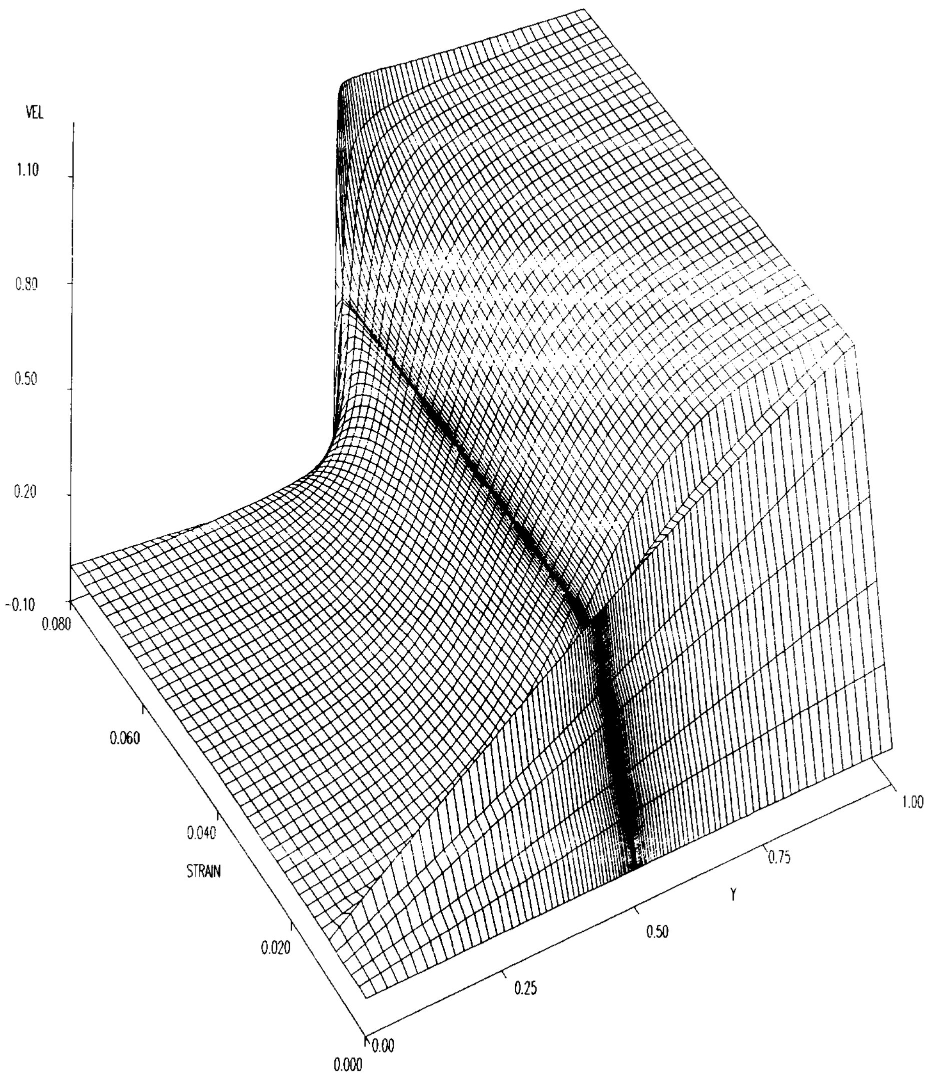

Fig. 2c. The evolution of the velocity field within the viscoplastic block being sheared at a nominal strain-rate of 1500 sec^{-1} for tungsten alloy.

Table 1. Data for different materials

Material	σ_0 (MPa)	$\bar{\rho}$ (kg/m^3)	θ_m (°C)	μ (GPa)	c (J/kg°C)	k (W/m°C)	$\bar{A}$ (MPa)	$\bar{B}$ (MPa)	D	n	α ($\times 10^{-3}$)	β ($\times 10^{-3}$)
OFHC copper	69	8,960	1,083	42	383	386	69	106	0.027	0.32	2.955	7.415
Cartridge brass	62	8,520	916	41	385	111	62	186	0.007	0.34	3.127	2.223
Nickel 200	138	8,900	1,453	80	446	90	138	234	0.008	0.32	1.467	1.495
Armco IF iron	76	7,890	1,538	76	452	73	76	196	0.028	0.25	2.362	1.349
Carpenter electric iron	193	7,890	1,538	78	452	73	193	109	0.028	0.43	0.930	1.349
1006 steel	200	7,890	1,538	80	452	73	200	129	0.022	0.36	0.898	1.349
2024-T351	152	2,770	502	28	875	119	152	202	0.015	0.34	0.415	3.237
7039 aluminum	193	2,770	604	28	875	149	193	157	0.01	0.41	0.327	4.053
Low alloy steel	455	7,840	1,520	76	477	38	455	237	0.006	0.37	0.392	0.670
S-7 tool steel	883	7,750	1,490	117	477	40	883	248	0.012	0.18	0.20	0.713
Tungsten alloy	862	17,000	1,450	133	134	75	862	94	0.016	0.12	0.449	0.217
Depleted uranium	621	18,600	1,200	58	117	28	621	561	0.007	0.25	0.681	0.848

been shown by, amongst others, BATRA [1989], the effect of inertia forces becomes somewhat noticeable when $\alpha = O(10^{-3})$ or higher. Thus, inertia forces will affect most the deformations of the block when it is made of Cartridge brass or OFHC copper, and least when the material is S-7 tool steel. The effect of thermal conductivity, if any, will show up most for OFHC copper, and least for the tungsten alloy.

Figures 2, 3, and 4 show solution surfaces for OFHC copper, S-7 tool steel, and tungsten alloy depicting, respectively, the evolution of the velocity, shear stress, and temperature rise within the specimen. The dark lines in these figures near the specimen center denote the region where a majority of nodes in the finite element mesh are concentrated. The three stages of the localization phenomenon, as reported by MARCHAND and DUFFY [1988] based on their experimental observations of torsion tests on an HY-100 steel, are evident in the velocity plots of Fig. 2. After the initial transients have died out, the velocity field in the block varies almost linearly, implying thereby that its deformations

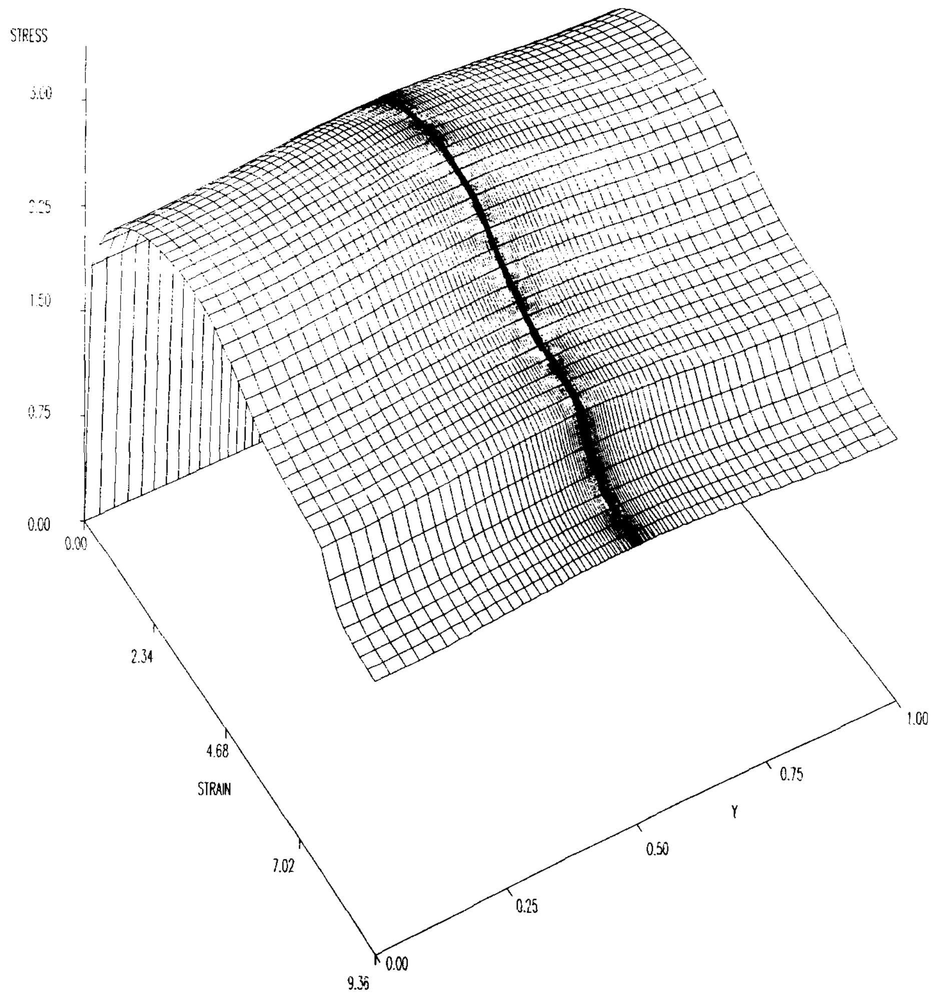

Fig. 3a. The solution surface for the shear stress for the viscoplastic block being sheared at a nominal strain-rate of 1500 sec^{-1} for OFHC copper. (*Figure continued*)

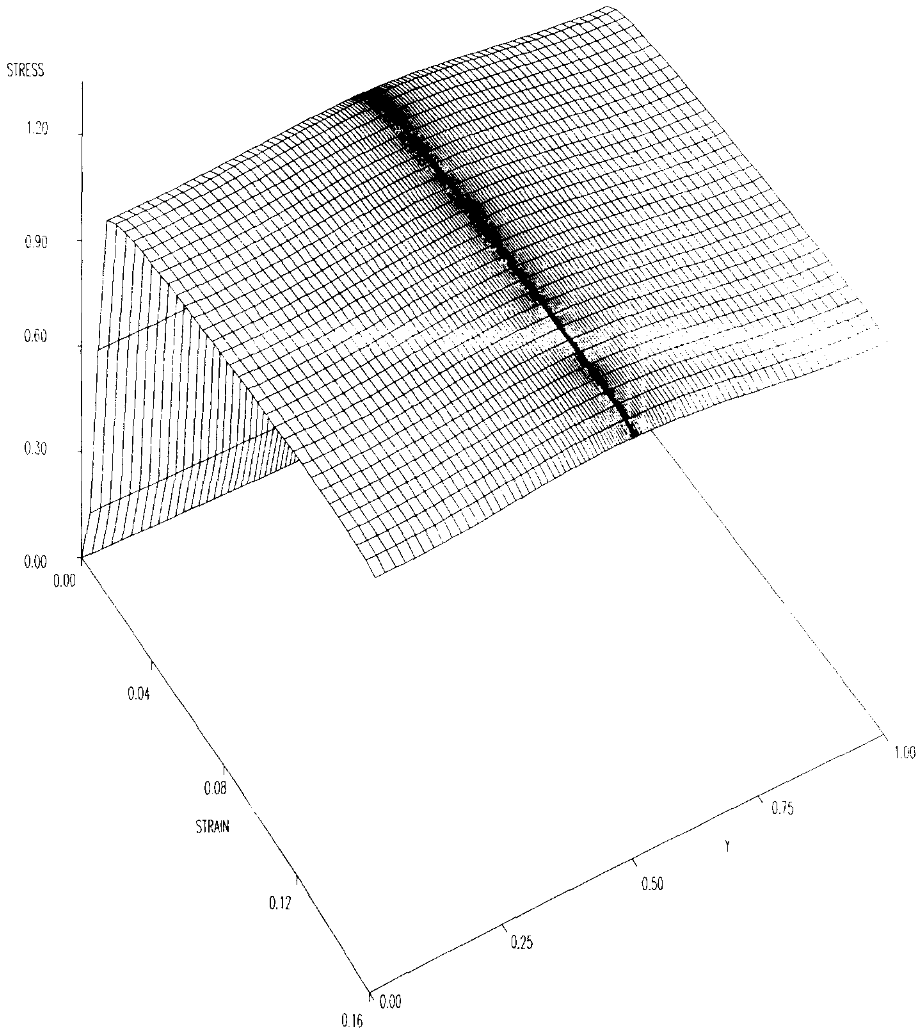

Fig. 3b. The solution surface for the shear stress for the viscoplastic block being sheared at a nominal strain-rate of 1500 sec^{-1} for S-7 tool steel.

are nearly homogeneous. Around the instant the stress attains its maximum value, the velocity field ceases to be linear, and the deformations of the block become nonhomogeneous. A sharp discontinuity in the velocity field develops *much later*, indicating the initiation of a shear band. For OFHC copper, S-7 tool steel, and tungsten alloy, the ratio of the average strain when a shear band initiates to the average strain at which the shear stress attains its peak value equals 2.13, 1.7, and 3.03, respectively. The discontinuity in the velocity field across the shear band as asserted by Tresca [1878] and Massey [1921] corresponds in our computations to the severe increase in the speed of the material particles across the shear band because, in our work, the velocity field is forced to stay continuous throughout the region under study. Batra [1989], by comparing the numerical solution of the full set of equations with those in which inertia effects are ne-

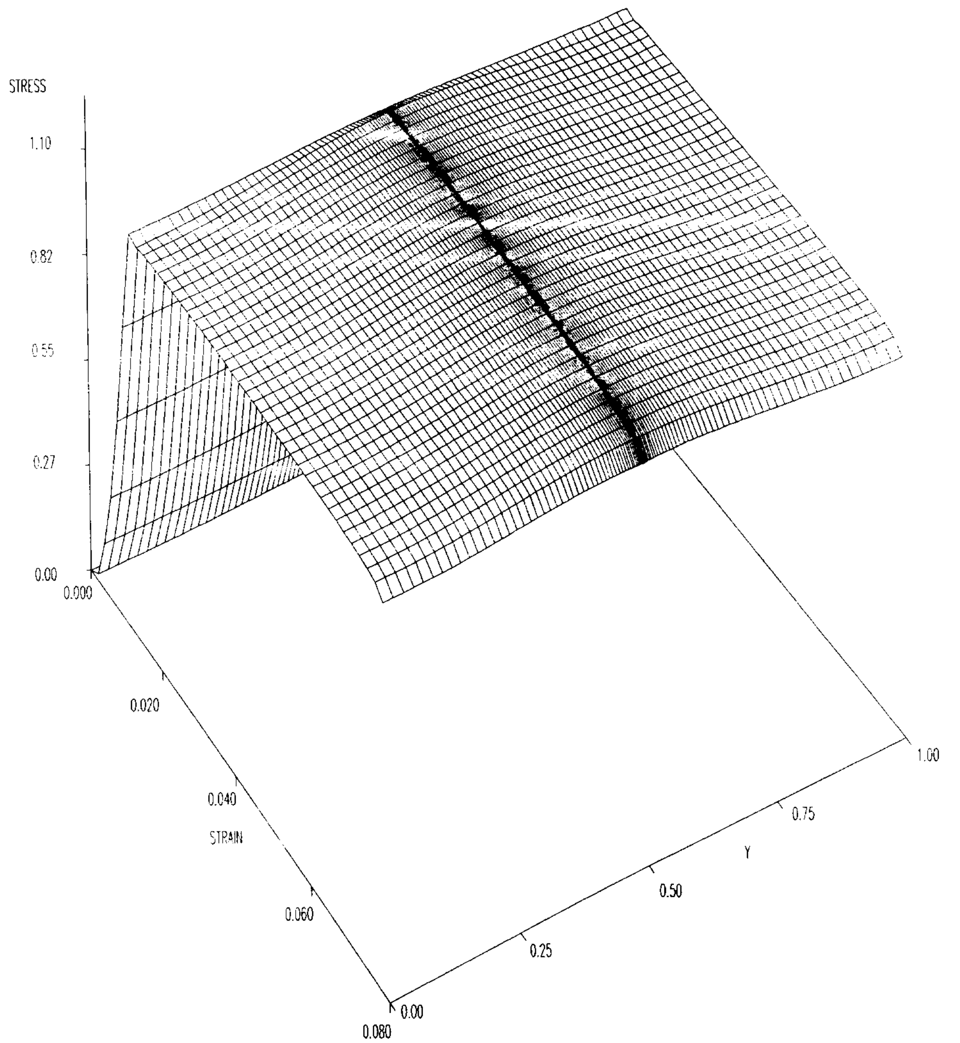

Fig. 3c. The solution surface for the shear stress for the viscoplastic block being sheared at a nominal strain-rate of 1500 sec^{-1} for tungsten alloy.

glected, showed that the effect of the inertia force is to delay the initiation of the localization phenomenon. The effect of the higher inertia force for copper manifests itself in the asymmetry of the velocity field about the center line, once the localization has initiated. Recall that the end $y = 0$ is kept fixed, and the velocity is prescribed at the end $y = 1$. Whereas for copper, the shear stress drops gradually, for S-7 tool steel and the tungsten alloy, the drop in shear stress is hardly noticeable till the deformations begin to localize. Then, the shear stress drops rapidly. This is not shown in the figure because soon after the rapid drop in the stress occurs, the numerical computations become unstable in the sense that the stress distribution within the specimen exhibits oscillatory behavior. The effect of higher thermal conductivity for copper is evident in the plots of the temperature distribution given in Fig. 4. For tungsten alloy and S-7 tool steel, the

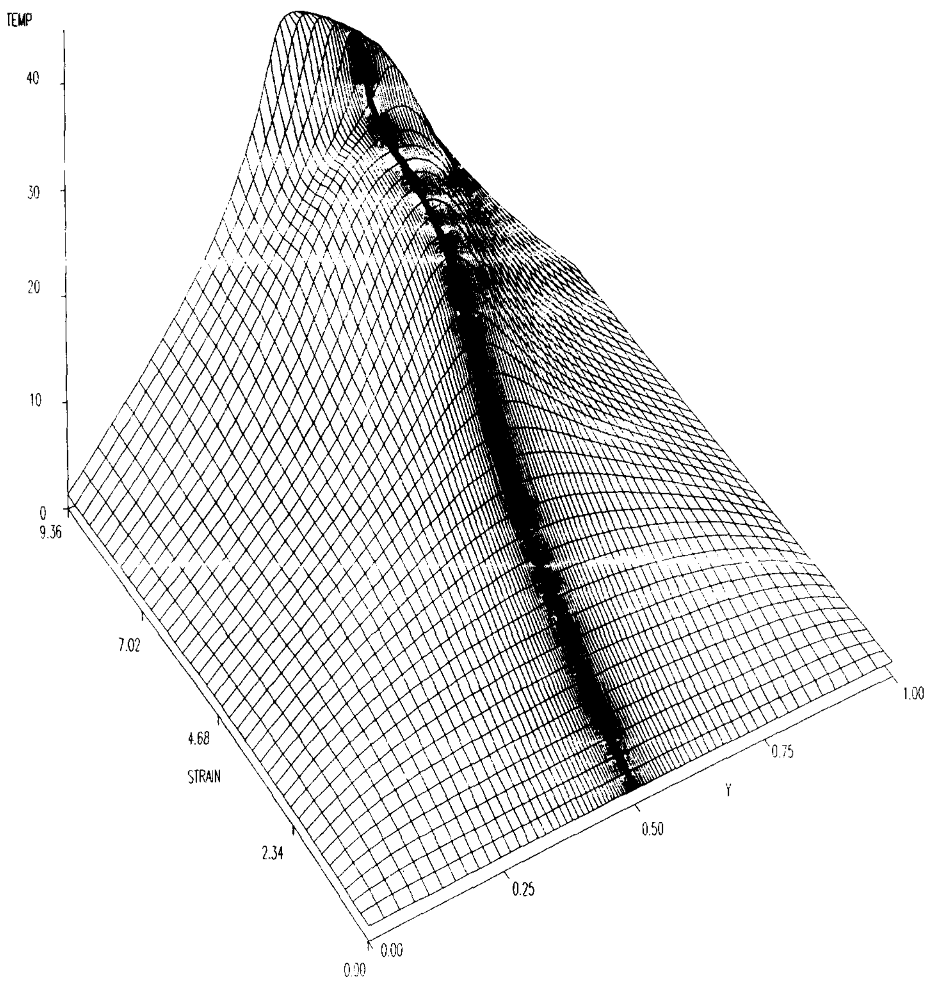

Fig. 4a. The solution surface for the temperature in a viscoplastic block being sheared at a nominal strain-rate of 1500 sec^{-1} for OFHC copper. (*Figure continued*)

temperature gradient near the specimen center is very steep; that for copper is gradual because more of the heat generated near the central severely deformed region is conducted outward. Also, once the localization has initiated, the temperature rises slowly near the specimen center for copper, but extremely rapidly for the tungsten alloy and S-7 tool steel. The plots of the plastic strain look very similar to that of temperature, and are not included herein. The plots of temperature suggest that wider bands form for copper as compared to those for S-7 tool steel and tungsten alloy.

Marchand and Duffy [1988] measured plastic strain at a point from the deformed position of a straight line initially parallel to the axis of the test specimen. As alluded to in the introduction, their experimental observations indicate that the shear strain localization phenomenon consists of three stages. In the first stage, the deformation stays homogeneous. Stage two, stipulated to initiate when the shear stress attains its peak value, involves nonhomogeneous deformations of the block. In stage three, the shear

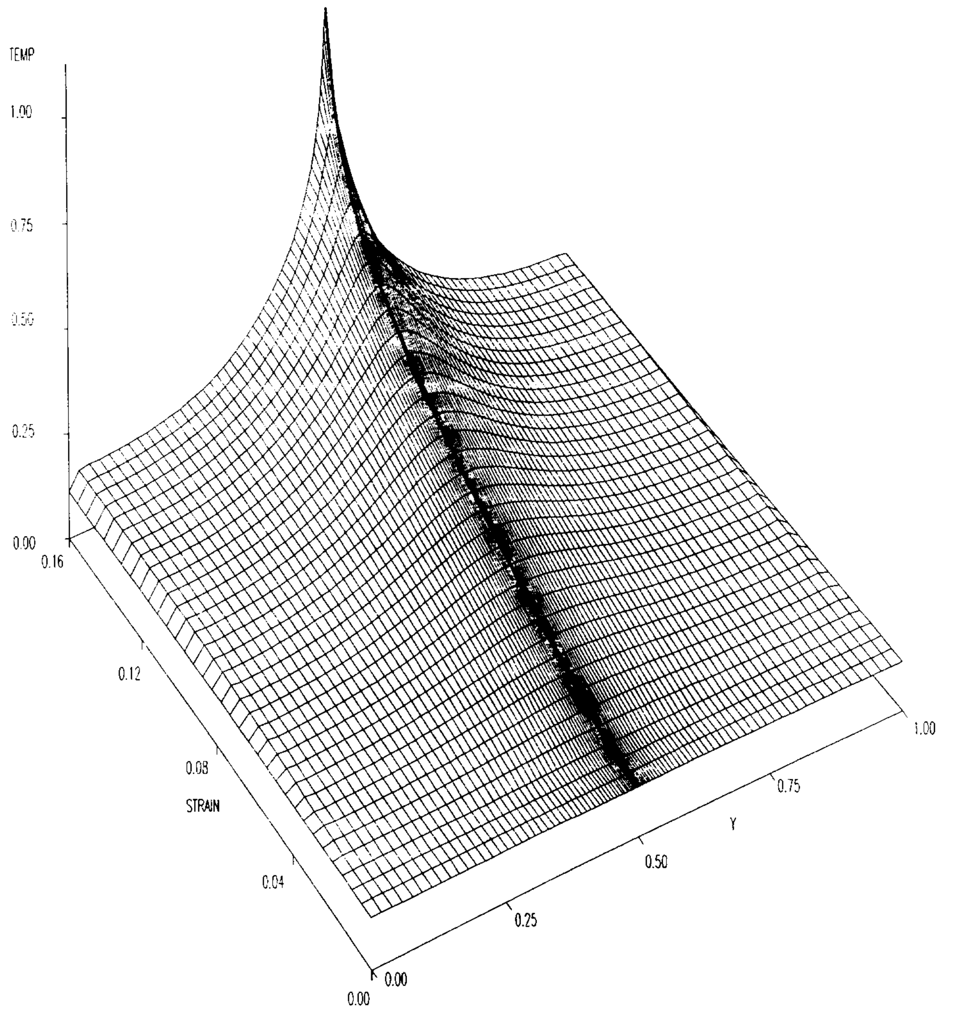

Fig. 4b. The solution surface for the temperature in a viscoplastic block being sheared at a nominal strain-rate of 1500 sec^{-1} for S-7 tool steel.

stress drops precipitously and the severely deforming region narrows down considerably. In order to see when stages two and three initiate in the materials studied herein, we have plotted in Fig. 5 the deformed positions of an initially vertical line when the shear stress s attains the peak values s_{max}, and when s equals 0.95 s_{max}, 0.90 s_{max}, 0.85 s_{max}, 0.80 s_{max}, and either 0.75 s_{max} (for less ductile materials) or 0.60 s_{max} (for ductile materials). We note that this line corresponds to one of the axial lines in the grid used by Marchand and Duffy [1988] to find the plastic strain at a point. For depleted uranium, the deformed positions of the line are shown for $s/s_{max} = 1.0$, 0.998, 0.996, 0.994, 0.992, and 0.990. In this case, the localization of the deformation in the central region is not evident because the shear stress did not drop much. These plots vividly reveal that the deformation has become nonhomogeneous by the time the peak shear stress occurs, possibly because of the nonuniform thickness of the specimen. Except for cop-

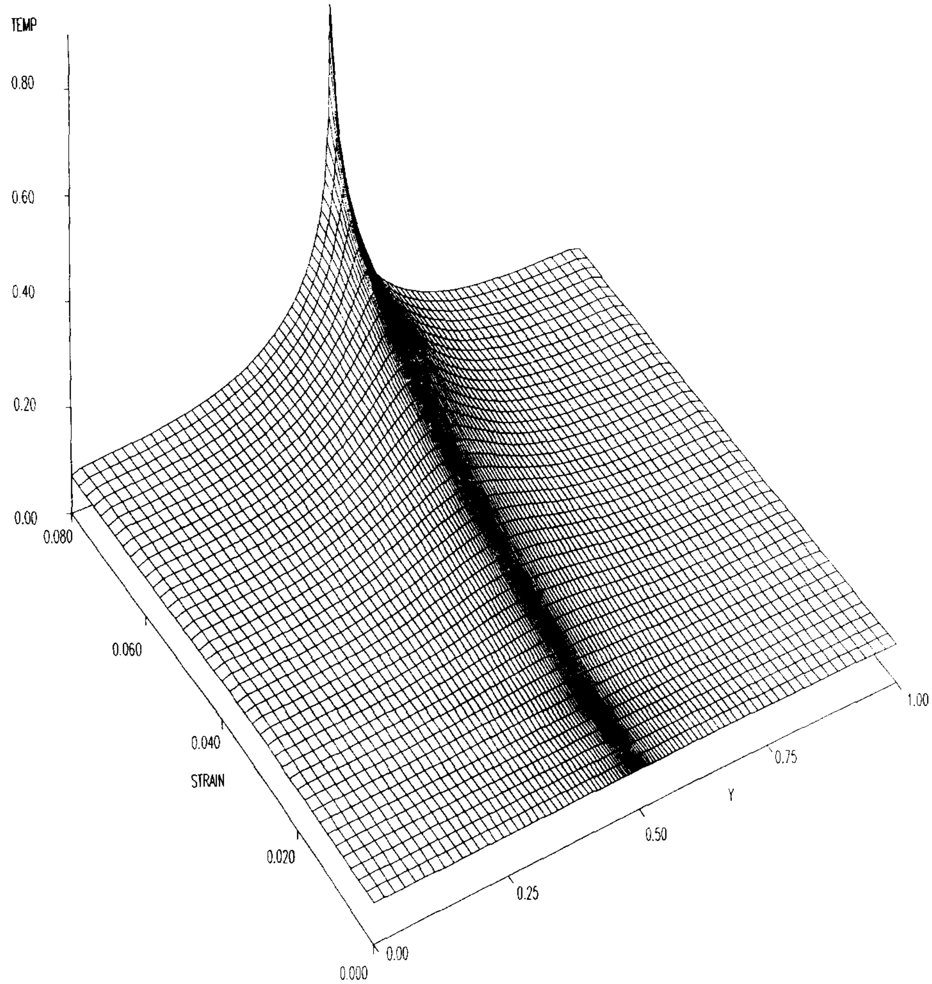

Fig. 4c. The solution surface for the temperature in a viscoplastic block being sheared at a nominal strain-rate of 1500 sec^{-1} for tungsten alloy.

per, the deformation is nonhomogeneous all along the specimen length. For copper, the central region of nonhomogeneous deformation is surrounded on either side by virtually uniformly deforming regions. For all of the materials studied, except for depleted uranium, cartridge brass and the low alloy steel, the deformation at the center increases sharply during the time the shear stress there drops from 0.90 s_{max} to 0.85 s_{max}. During the subsequent drop of the shear stress, the deformation at the center continues to increase at the accelerated pace, and the severely deforming region continues to narrow down in size. Therefore, one might say that the band begins to grow in earnest when the shear stress has dropped to 90% of its maximum value. The displacement in the direction of shearing of a point at the band center is small for cartridge brass, Nickel 200, low alloy steel, 7039 aluminum, and the depleted uranium. For all these materials the value of D is quite low, suggesting that the strain-rate sensitivity of the material may influence the growth of the band after it has initiated.

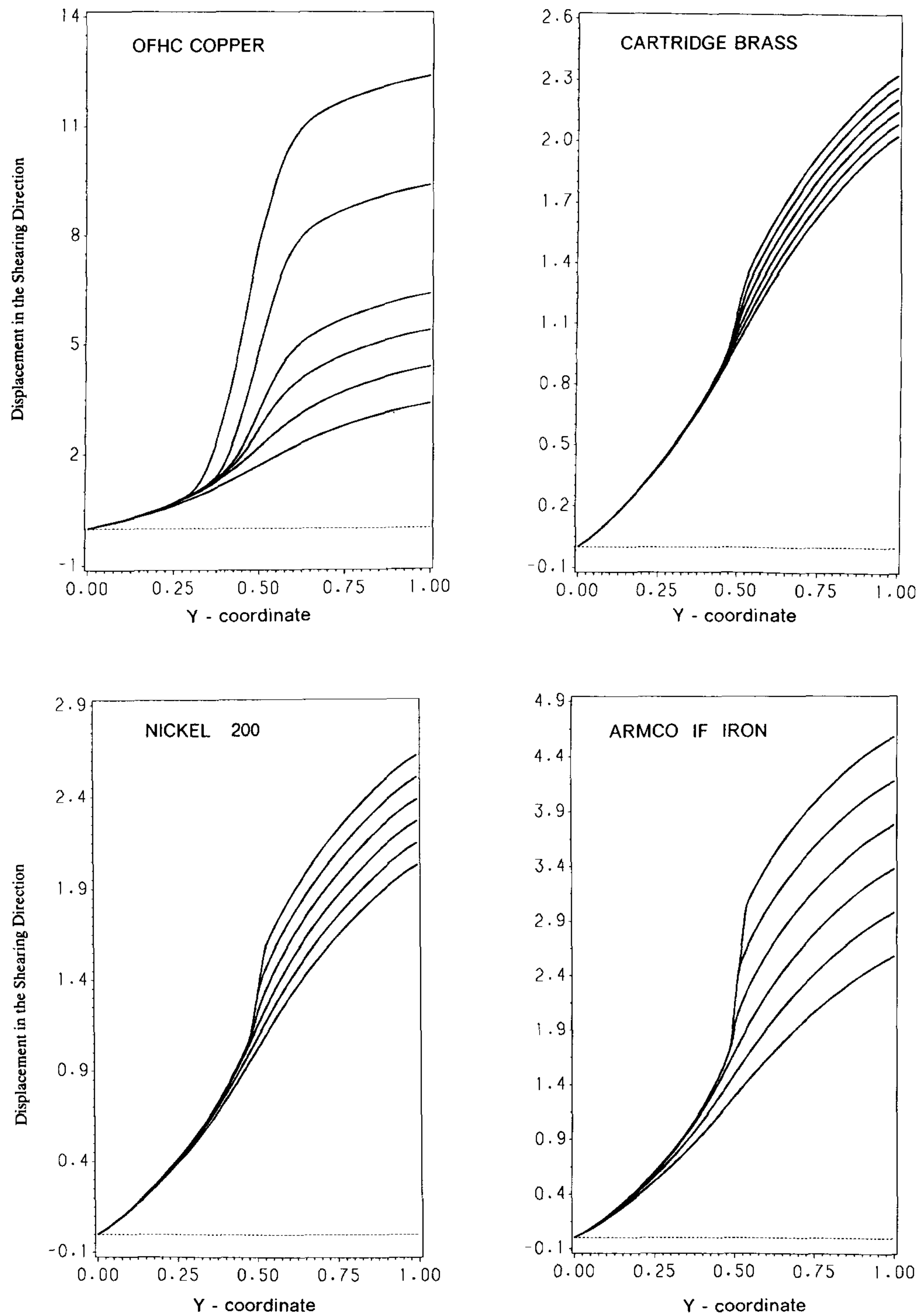

Fig. 5. Deformed shapes of an initially straight line for the six ductile materials at $s/s_{max} = 1.0, 0.95, 0.90, 0.85, 0.80$, and 0.60; for the six less ductile materials except depleted uranium at $s/s_{max} = 1.0, 0.95, 0.90, 0.85, 0.80$, and 0.75; for depleted uranium at $s/s_{max} = 1.0, 0.998, 0.996, 0.994, 0.992$, and 0.990. (*Figure continued*)

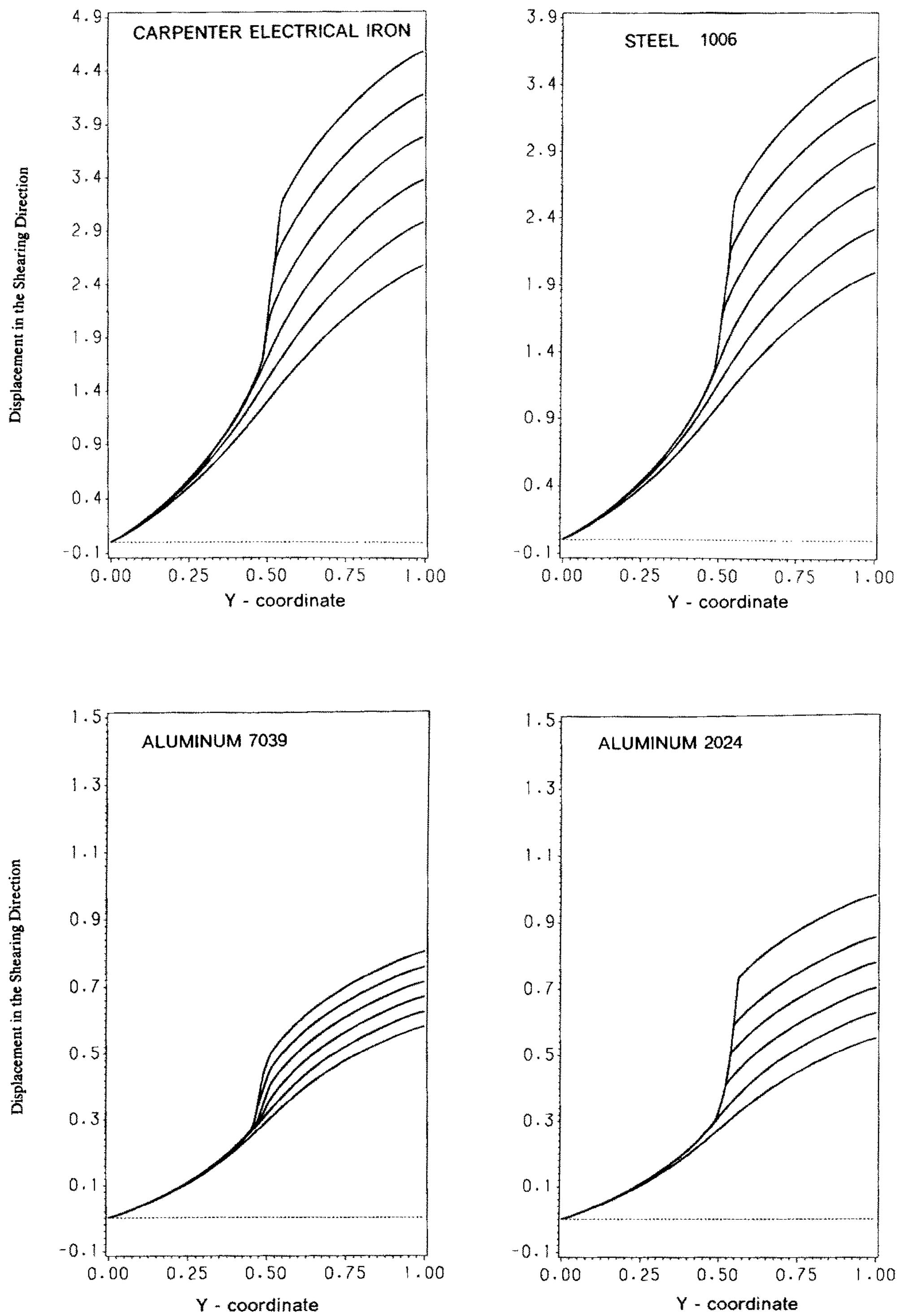

Fig. 5. continued.

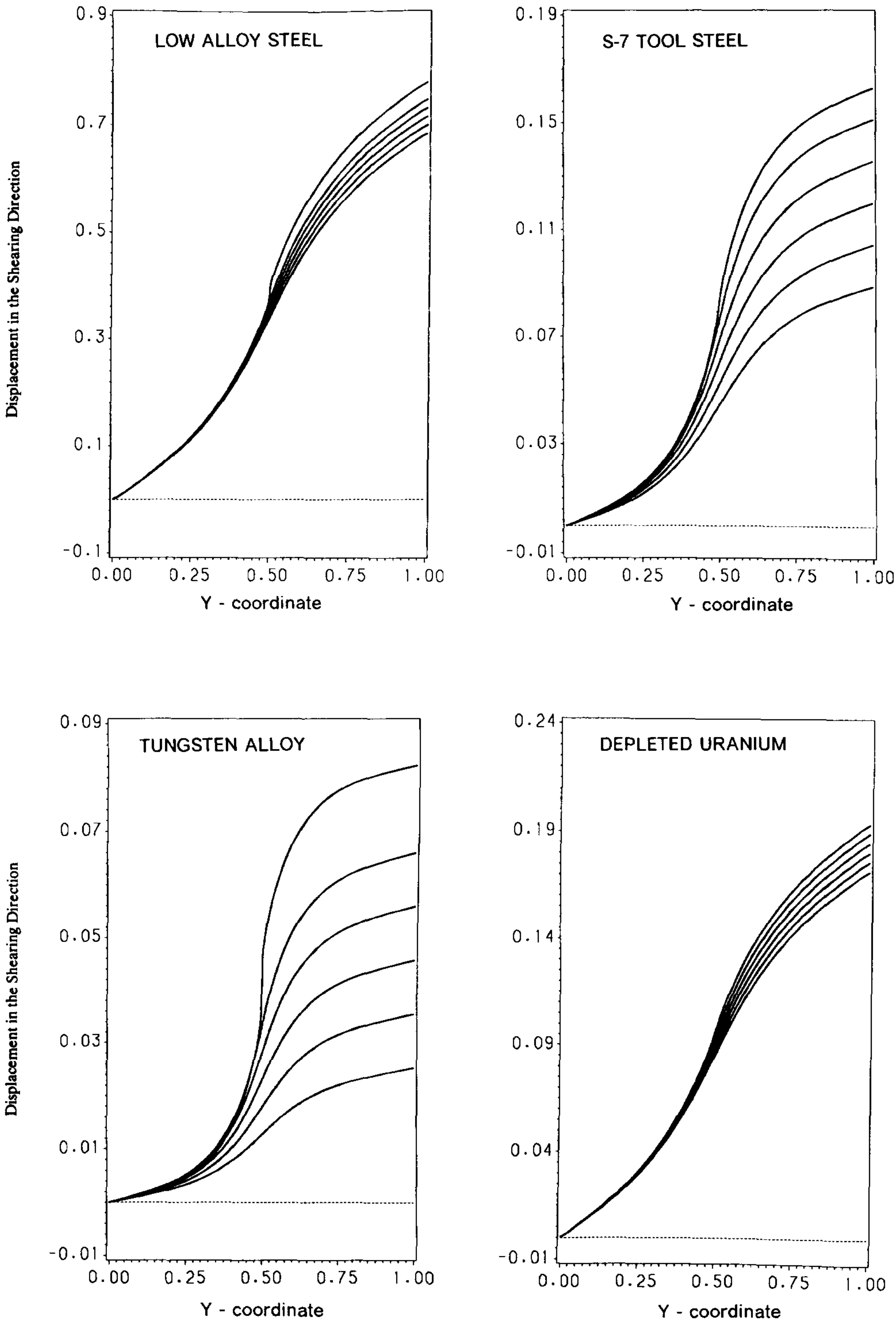

Fig. 5. continued.

Because of the intense deformations at and near the center of the band, a considerable amount of heat is generated there, and the temperature rises significantly. Figure 6 depicts the homologous temperature, defined as the ratio of the absolute temperature of a material particle to the melting temperature of the material, at the band center as the shear stress there drops. Note that s/s_{max} represents a distorted time scale during the interval in which the shear stress is dropping. For example, the shear stress drops from s_{max} to 0.95 s_{max}, say, in 100 μs, but it drops from 0.95 s_{max} to 0.70 s_{max} in only 4 or 5 μs. By the time the shear stress drops to 0.75 s_{max}, the homologous temperature at the band center has reached nearly 0.7. For each of the six ductile materials, the curves are nearly parallel to each other, and all six curves lie in a narrow band. For the less ductile materials, the temperature varies over a wider range for the same value of s/s_{max}.

It is clear from the results plotted in Fig. 5 that the width of the severely deformed region depends upon how far the shear stress has dropped from its maximum value. Since we do not have any failure criterion included in our work, it is hard to decide when the band has fully developed. MARCHAND and DUFFY [1988] defined the band width as the width of the region over which plastic strain stays constant and equals the maximum value observed in a test. If we use herein their definition of the band width, it would come out to be zero, since the peak value of the computed plastic strain occurs at one point only. Accordingly, we define the band width as the width of the region surrounding the band center over which the plastic strain differs from its peak value by less than 5%. The plots of the deformed position of an initially straight line given in Fig. 5 indicate that the band has essentially developed by the time $s = 0.85\ s_{max}$. Hereafter, we

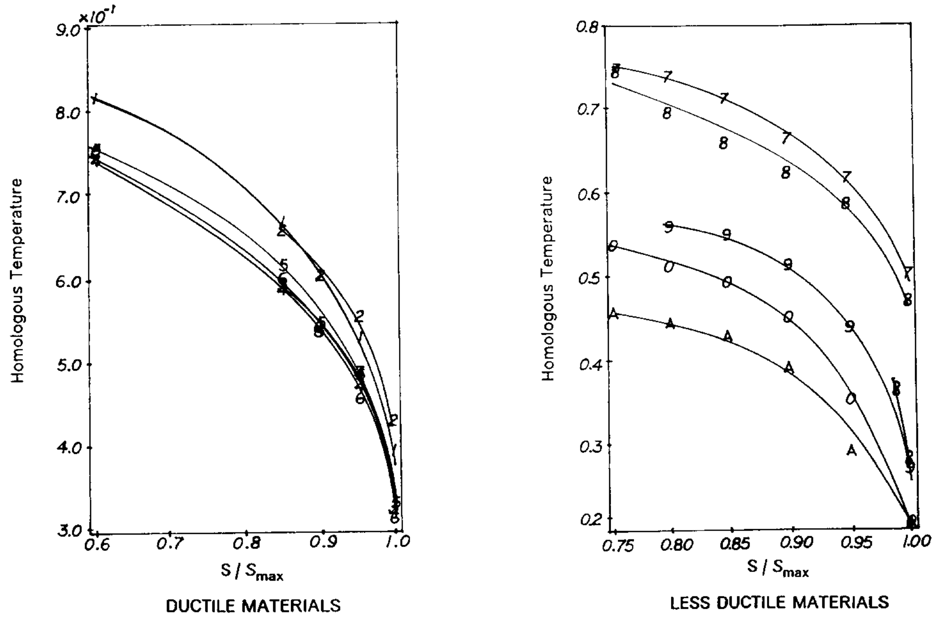

Fig. 6. The evolution of the homologous temperature at the band center during the time shear stress is collapsing (1 - copper, 2 - cartridge brass, 3 - Nickel 200, 4 - Armco IF iron, 5 - carpenter electric iron, 6 - 1006 steel, 7 - 2024 aluminum, 8 - 7039 aluminum, 9 - low alloy steel, 0 - S-7 tool steel, A - tungsten alloy, B - depleted uranium).

find the band width when $s/s_{max} = 0.85$. The band width is plotted against the thermal length ℓth, defined as,

$$\ell th = (k/(\rho c \dot{\gamma}_0))^{1/2} \times 10^6 \ \mu m$$

in Fig. 7. The scatter in the data indicates that there is no simple correlation between the two. For the Armco IF iron, Carpenter iron, and 1006 steel considered, the computed band width is different, even though the values of the thermal conductivity and the thermal length are the same.

MARCHAND and DUFFY [1988] showed that

$$\gamma_{loc} = a\lambda^b, \tag{19}$$

where γ_{loc} is the plastic strain at the band center, and λ is the band width in microns, fits the experimental data for HY-100 steel well when $a = 125.8$ and $b = -0.867$. For the 12 materials studied herein, values obtained for a and b when we fit the curve by the least squares method to the computed data are shown in Table 2.

The fitted curves and the computed data points are shown in Fig. 8. The Armco IF iron, Carpenter electric iron, and the 1006 steel show different rates of shear band development, in spite of their having the same value of the thermal conductivity and the

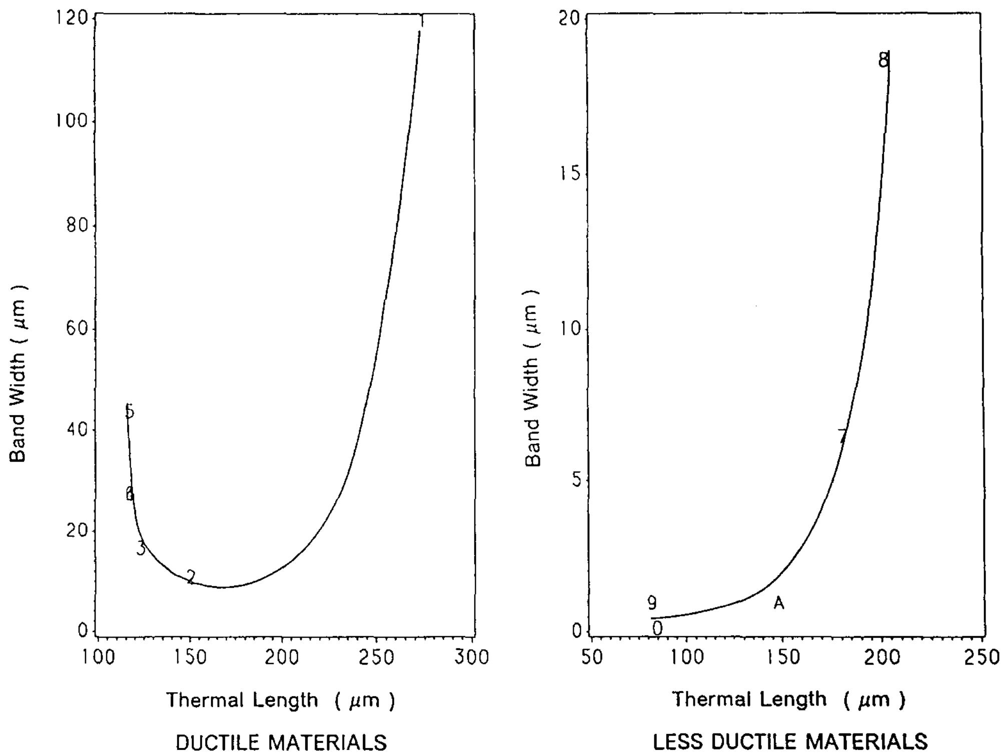

Fig. 7. The dependence of the band width upon the thermal length.

Table 2. Values for a and b for the twelve materials studied

Material	Values of a	b
OFHC copper	10057.0	−1.30
Cartridge brass	13.93	−0.261
Nickel 200	27.58	−0.382
Armco IF iron	45.19	−0.382
Carpenter electric iron	78.65	−0.492
1006 steel	61.89	−0.499
7039 aluminum	9.948	−0.416
2024 aluminum	5.663	−0.324
Low alloy steel	6.116	−0.291
S-7 tool steel	2.250	−0.378
Tungsten alloy	2.496	−0.581
Depleted uranium	0.954	−0.197

thermal length. It is rather difficult to find a correlation between the values of a and b and of the material parameters α, β, m, n, and D.

We now examine the effect of the defect size on the deformations of the 12 materials. In Fig. 9a, we have plotted the dependence of the critical strain ϵ_{cr}, defined as the value of the nominal strain when the shear stress attains its maximum value, upon the percentage decrease δ in the thickness of the specimen at the center relative to that at the edges. The range 3.54% to 10% of the values of δ considered herein was suggested by a local mechanic, well experienced in machining. The straight lines, fitted by the least squares method, through the computed data points have equations

$$\epsilon_{cr} = \epsilon_{cr}^0 + \nu(\log \delta + 1), \qquad 0.0354 \le \delta \le 0.10$$

where ϵ_{cr}^0 is the critical strain at $\delta = 0.10$. Values of ϵ_{cr}^0 and ν for the twelve materials are listed in Table 3.

Table 3. Values of ϵ_{cr}^0 and ν for the twelve materials studied

Material	ϵ_{cr}^0	ν
OFHC copper	3.1243	−0.626
Cartridge brass	1.7784	−0.741
Nickel 200	1.8408	−0.901
Armco IF iron	2.3691	−1.010
Carpenter electric iron	2.2457	−1.093
1006 steel	1.6918	−1.021
7039 aluminum	0.465	−0.361
2024 aluminum	0.454	−0.265
Low alloy steel	0.521	−0.534
S-7 tool steel	0.074	−0.074
Tungsten alloy	0.0215	−0.020
Depleted uranium	0.140	−0.141

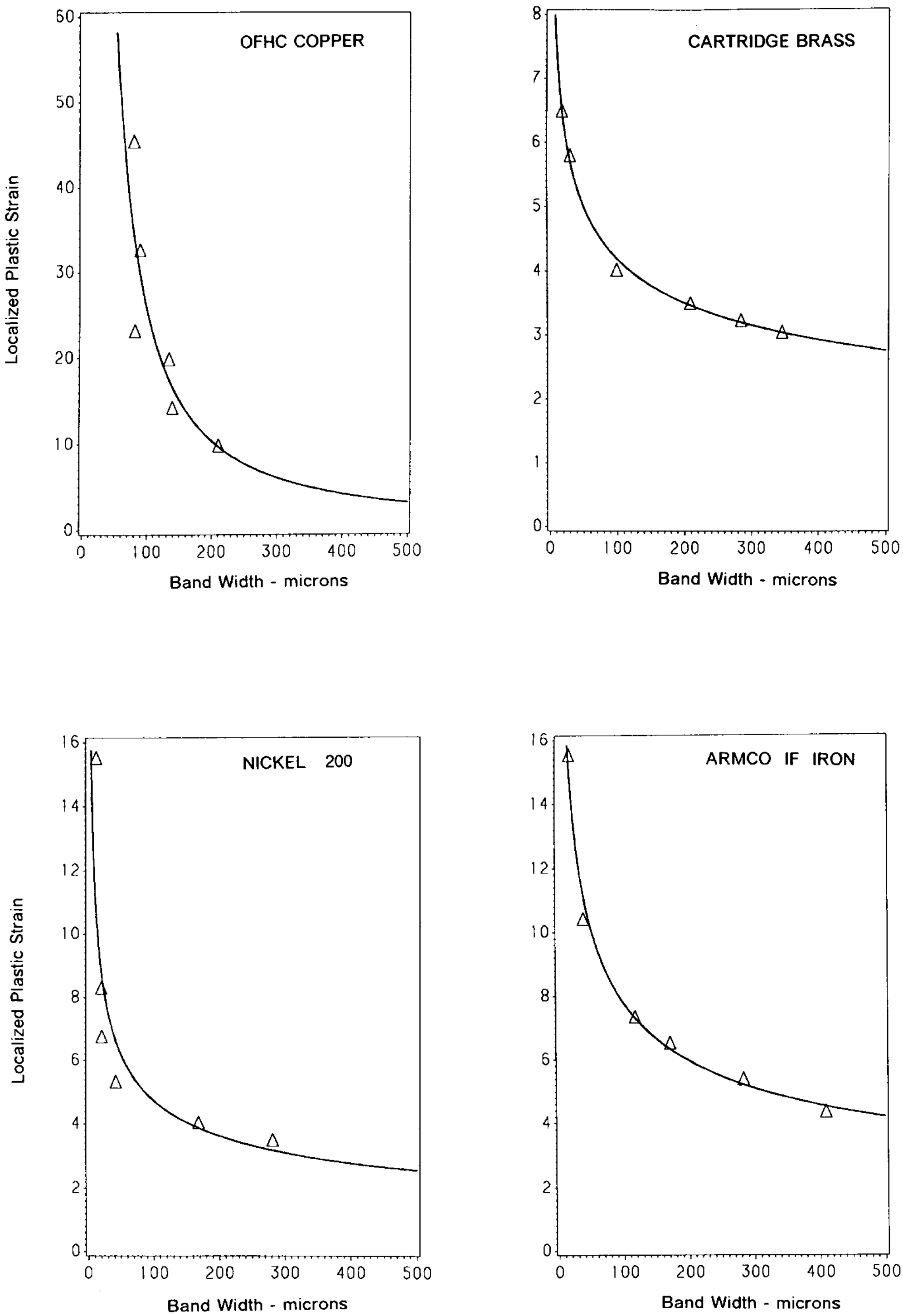

Fig. 8. Plastic strain at the band center vs. the band width. Triangles indicate the computed data points. (*Figure continued*)

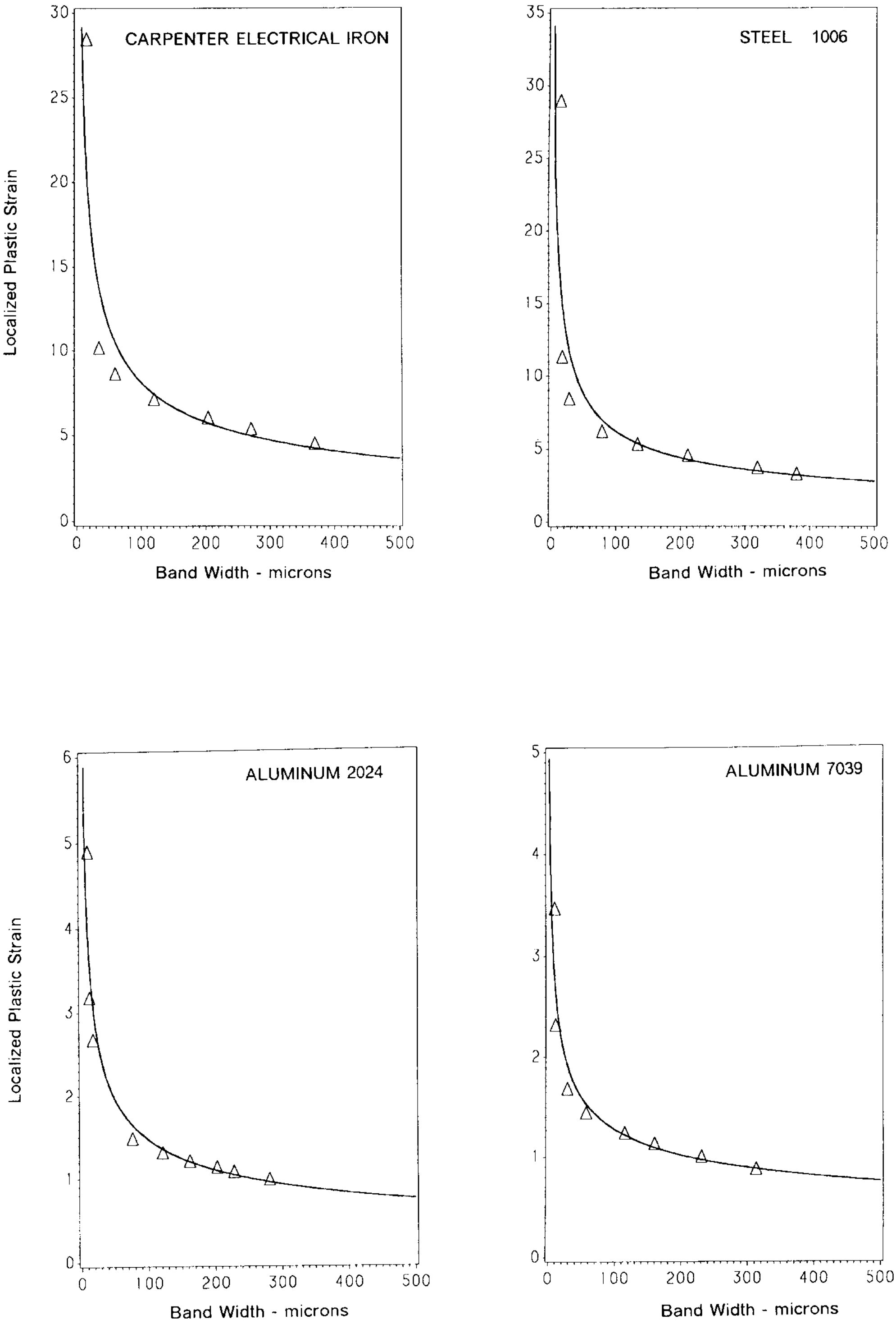

Fig. 8. continued.

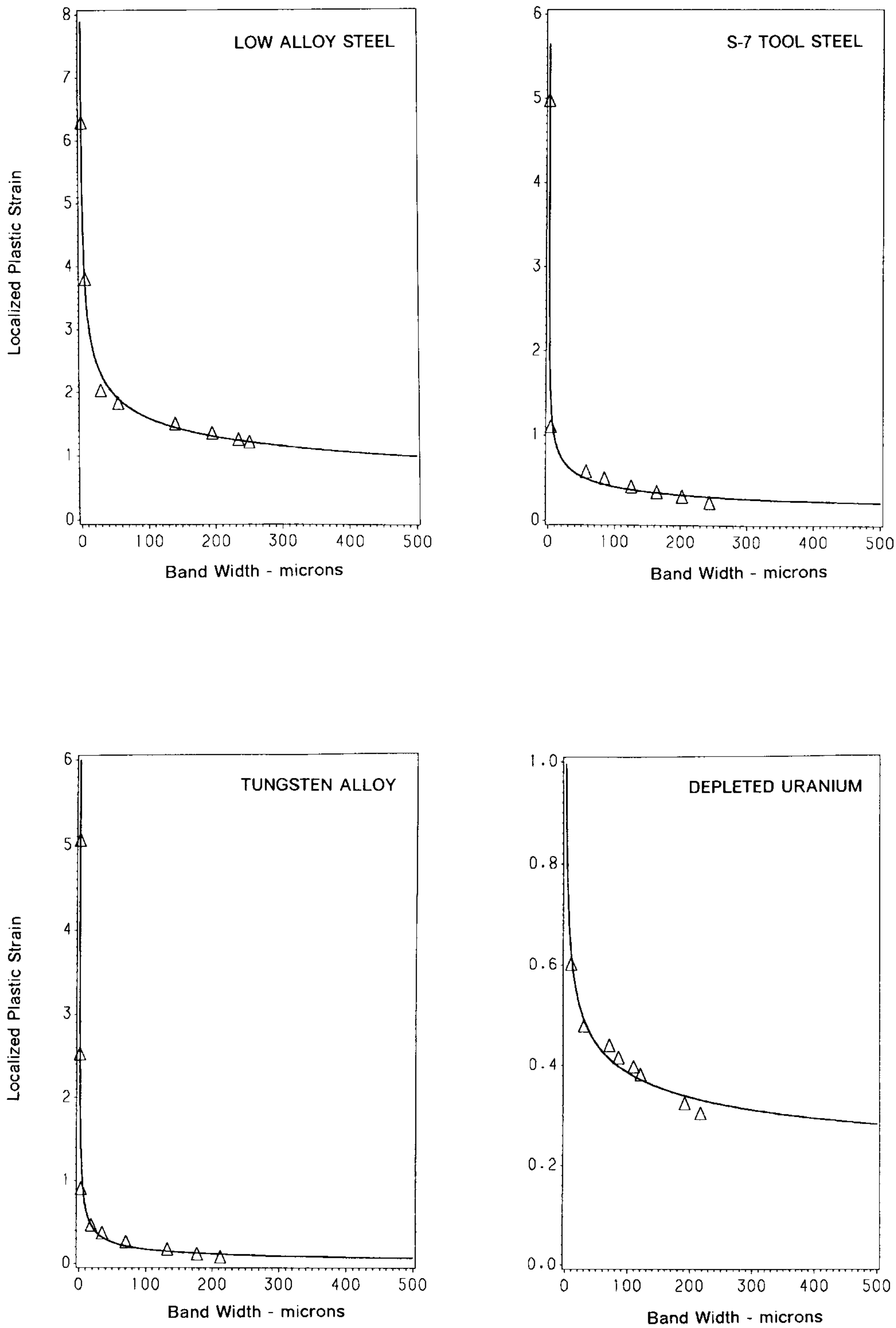

Fig. 8. continued.

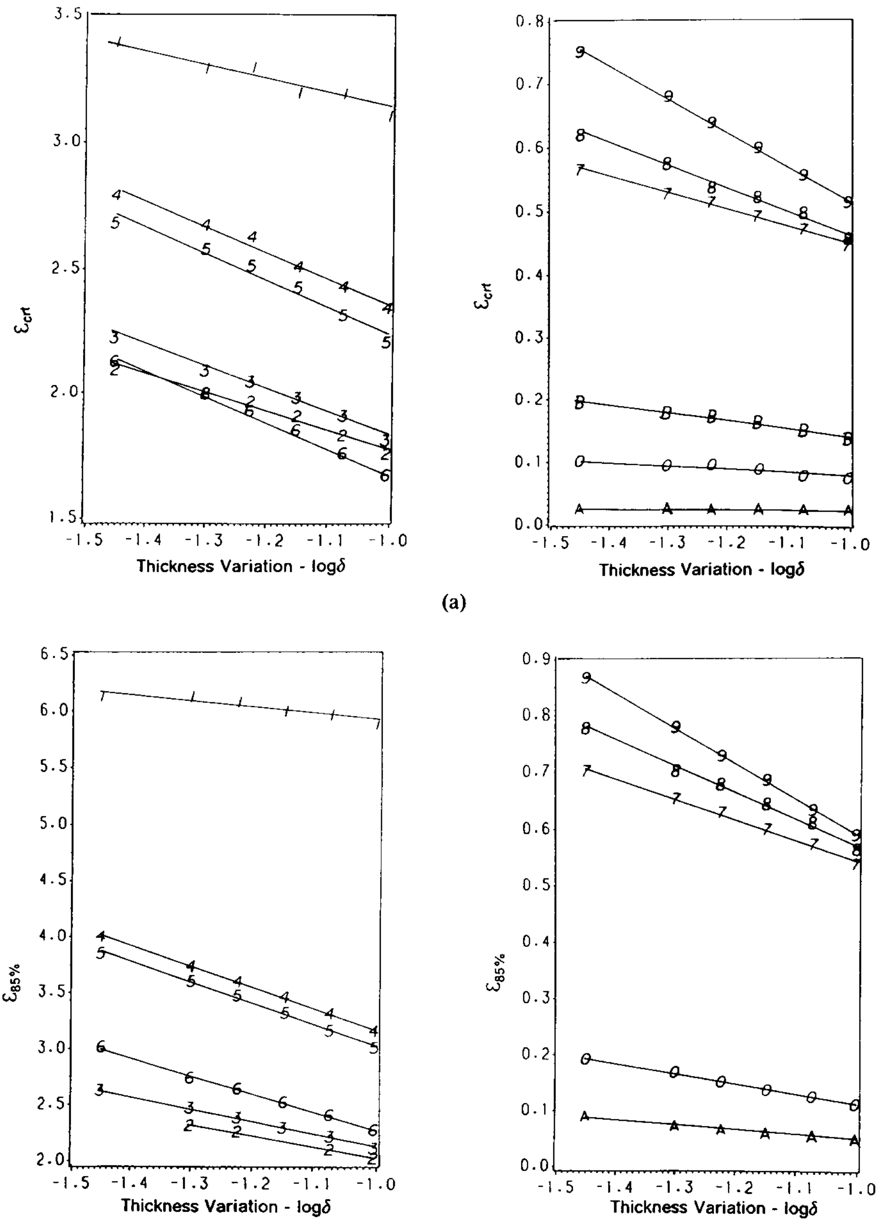

Fig. 9. Dependence of the nominal strain when (a) $s/s_{max} = 1.0$, and (b) $s/s_{max} = 0.85$ upon the defect size (see Fig. 6 caption for explanations).

The computed values of ϵ_{cr}^0 and ν for the six ductile materials are more than those for the six less ductile materials. Thus, the defect size influences more the value of the critical strain for ductile materials as compared to that for the less ductile materials studied herein. Figure 9b depicts the variation of the nominal strain at $s/s_{max} = 0.85$ with the defect size. The curves for the Armco IF iron, Carpenter electric iron, and the 1006 steel are parallel to each other. At $s/s_{max} = 0.85$, the computed data for all materials, except copper, lie on parallel straight lines. The distinguishing characteristics of the OFHC copper are its high ductility and thermal conductivity. The computed data when plotted as ϵ/ϵ_{cr} versus log δ at $s/s_{max} \simeq 0.95$, 0.90, and 0.85 did not exhibit any similarities for the

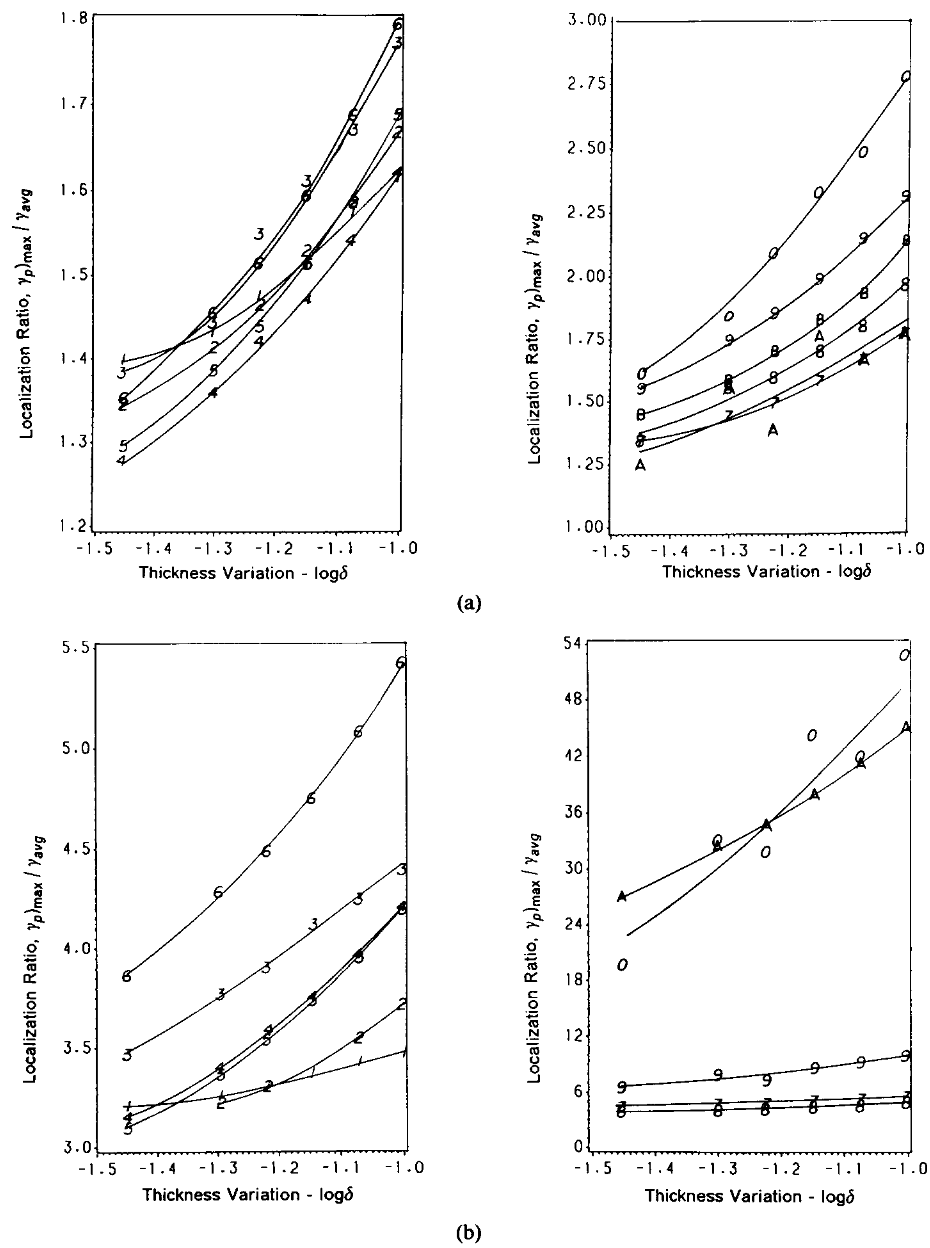

Fig. 10. Dependence of the localization ratio upon the defect size for (a) $s/s_{max} = 1.0$, and (b) $s/s_{max} = 0.85$ (see Fig. 6 caption for explanations).

12 materials. How the localization of the deformation depends upon the defect size is exhibited in Figs. 10a and 10b for $s/s_{max} \simeq 1.0$ and 0.85, respectively. The ordinate in these figures equals the ratio of the maximum shear strain within the severely deforming region to the nominal strain in the specimen. This localization ratio depends strongly upon log δ; larger defects result in more severe localization of the deformation for the

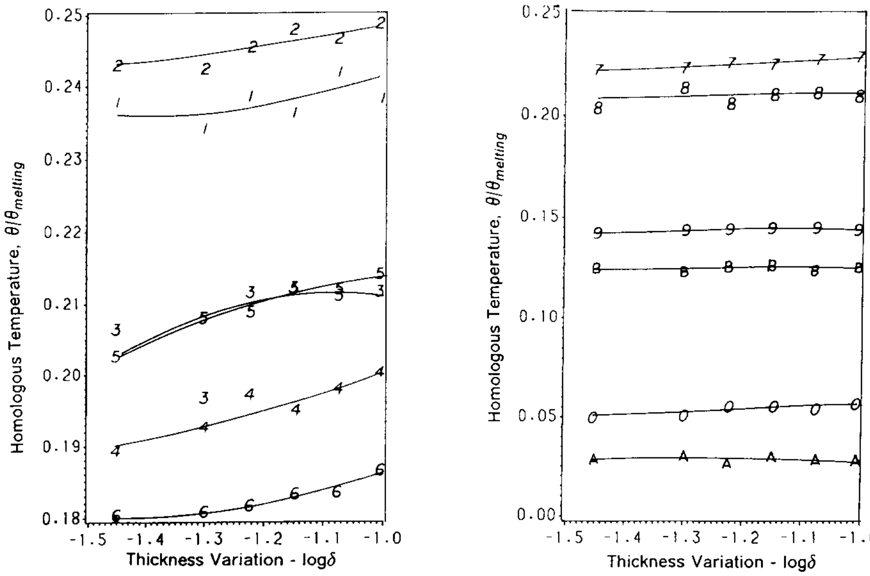

(a)

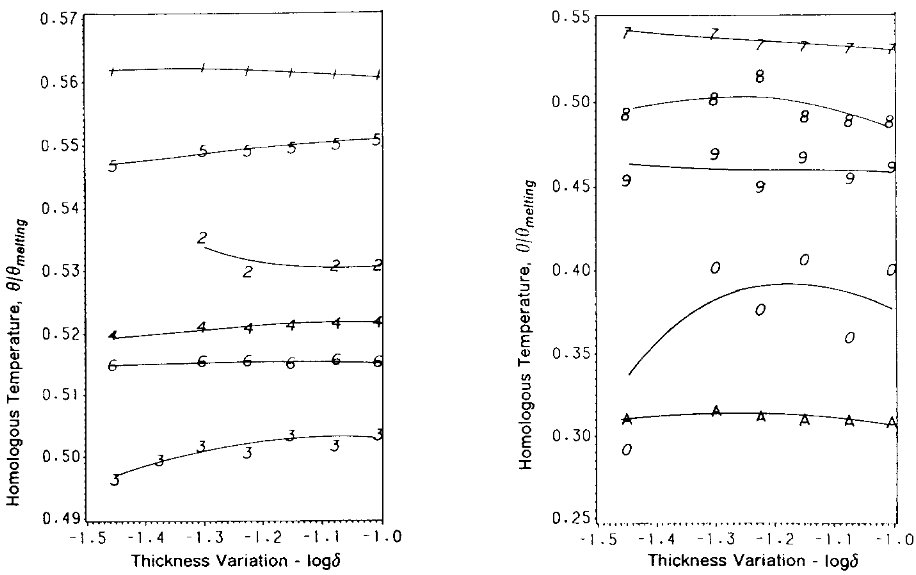

(b)

Fig. 11. Dependence of the homologous temperature at the band center upon the defect size when (a) s/s_{max} = 1.0, (b) s/s_{max} = 0.85 (see Fig. 6 caption for explanations).

same value of s/s_{max}. That is, the defect size affects not only the nominal strain when a shear band initiates, but also the growth of the shear band. For $s/s_{max} = 1.0$, the curves for the six ductile materials and the six less ductile materials are essentially parallel to each other. However, this similarity disappears as the shear stress within the region of localization drops, except that the curves for the Armco IF iron, Carpenter electric iron, and the 1006 steel do stay parallel to each other, even through the drop of the shear stress. The homologous temperature versus log δ plots in Figs. 11a and 11b reveal that the homologous temperature is essentially independent of the defect size at $s/s_{max} = 1.0$ and 0.85. Note that the vertical scales in these figures are such that small differences in the values of the homologous temperatures are noticeably exaggerated.

IV. CONCLUSIONS

We have studied the initiation and growth of shear bands in a block undergoing overall simple shearing deformations at a nominal strain-rate of 1500 sec^{-1}. The ends of the block are presumed to be kept at a constant temperature, and the problem is solved for six ductile materials: OFHC copper, Cartridge brass, Nickel 200, Armco IF iron, Carpenter electric iron, and 1006 steel, and six less ductile materials: 7039 aluminum, 2024 aluminum, low alloy steel, S-7 tool steel, tungsten alloy, and depleted uranium. Among the principal findings, we mention the following. The deformations of the block become nonhomogeneous before the shear stress attains its maximum value. The Stage III of deformation stipulated by Marchand and Duffy begins when the shear stress has dropped to approximately 95% of its maximum value. The shear band begins to grow rapidly when the shear stress within the band has dropped to 90% of its peak value. The defect size affects noticeably the value of the nominal strain at which the shear stress becomes maximum. Larger defects result in more severe localization of the deformation for the same value of s/s_{max}. The defect size has very little effect on the value of the homologous temperature when $s = s_{max}$ and 0.85 s_{max}. In none of the materials studied herein was the drop in the shear stress at the band center so severe as to cause the emanation of an elastic unloading wave out of the band. Such an unloading wave was computed by Batra and Kim [1990] for a material that exhibited quite high thermal softening effects. The computed band width decreases with the thermal length; however, there is no simple correlation between the two.

Acknowledgements—This work was supported by the U.S. National Science Foundation Grant MSM 8715952 and the U.S. Army Research Office Contract DAAL03-88-K-0184 to the University of Missouri-Rolla. Some of the computations were performed on the NSF sponsored supercomputer center at Cornell University.

REFERENCES

1878 Tresca, H., "On Further Application of the Flow of Solids," Proc. Inst. Mech. Engr. **30**, 301.
1921 Massey, H.F., "The Flow of Metal During Forging," Proc. Manchester Assoc. Engineers, pp. 21–26.
1925 Farren, W.S., and Taylor, G.I., "The Heat Developed During Plastic Extrusion of Metal," Proc. R. Soc., **A107**, 422.
1944 Zener, C., and Hollomon, J.H., "Effect of Strain Rate on Plastic Flow of Steel," J. Appl. Phys., **15**, 22.
1964 Recht, R.F., "Catastrophic Thermoplastic Shear," ASME J. Appl. Mech., **31**, 189.
1972 Gear, C.W., "Numerical Initial Value Problems in Ordinary Differential Equations," Prentice Hall, Englewood Cliffs, NJ.
1978 Wulf, G.L., "The High Strain Rate Compression of 7039 Aluminum," Int. J. Mech., **20**, 609.
1979 Costin, L.S., Crisman, E.E., Hawley, R.H., and Duffy, J., "On the Localization of Plastic Flow in Mild Steel Tubes Under Dynamic Torsional Loading," Int. Phys. Conf. Ser. No. 47, pp. 90–100.
1979 Sulijoadikusumo, A.V., and Dillon, O.W., "Temperature Distribution for Steady State Axisymmet-

ric Extrusion with an Application to Ti-6Al-4V: Part 1, J. Thermal Stresses, **2**, 97; Part 2, *Ibid.*, **2**, 113; Part 3, *Ibid.*, **3**, 265.

1980 CLIFTON, R.J., "Material Response to Ultra High Loading Rates," NRC National Material Advisory Board (U.S.) Report 356.

1981 MOSS, G.L., "Shear Strain, Strain Rate and Temperature Changes in Adiabatic Shear Bands," in MEYER, M.A., and MURR, L.E. (eds.), Shock Waves and High Strain Rate Phenomenon in Metals, Plenum Press, New York, pp. 299–312.

1981 STAKER, M.R., "The Relation Between Adiabatic Shear Instability Strain and Material Properties," Acta Met., **29**, 683.

1982 MERZER, A.M., "Modeling of Adiabatic Shear Band Development from Small Imperfections," J. Mech. Phys. Solids, **30**, 323.

1983 HINDMARSH, A.C., "ODEPACK, A Systematized Collection of ODE Solvers," in STEPLEMAN, R.S., *et al.* (eds.), Scientific Computing, North-Holland, Amsterdam, pp. 55–64.

1983 JOHNSON, G.R., and COOK, W.H., "A Constitutive Model and Data for Metals Subjected to Large Strains, High Strain Rates and High Temperatures," Proc. 7th Int. Symp. Ballistics, The Hague, The Netherlands, pp. 1–7.

1983 JOHNSON, G.R., HOEGFELDT, J.M., LINDHOLM, V.S., and NAGY, A., "Response of Various Metals to Large Torsional Strain Over a Large Range of Strain Rates, Part I: Ductile Metals, Part II: Less Ductile Metals," ASME J. Eng. Materials Technol., **105**, 48.

1985 BURNS, T.J., "Approximate Linear Stability Analysis of a Model of Adiabatic Shear Band Formation," Quart. Appl. Math., **43**, 65.

1985 WRIGHT, T.W., and BATRA, R.C., "The Initiation and Growth of Adiabatic Shear Bands," Int. J. Plasticity, **1**, 205.

1986a LEMONDS, J., and NEEDLEMAN, A., "Finite Element Analyses of Shear Localization in Rate and Temperature Dependent Solids," Mechs. Materials, **5**, 339.

1986b LEMONDS, J., and NEEDLEMAN, A., "An Analysis of Shear Band Development Incorporating Heat Conduction," Mechs. Materials, **5**, 363.

1987 BATRA, R.C., "The Initiation and Growth of, and the Interaction Among Adiabatic Shear Bands in Simple and Dipolar Materials," Int. J. Plasticity, **3**, 75.

1987 HARTLEY, K.A., DUFFY, J., and HAWLEY, R.H., "Measurement of the Temperature Profile During Shear Band Formation in Steels Deforming at High Strain Rates," J. Mechs. Phys. Solids, **35**, 283.

1987 JOHNSON, W., "Henri Tresca as the Originator of Adiabatic Heat Lines," Int. J. Mech. Sci., **29**, 305.

1987 MOLINARI, A., and CLIFTON, R.J., "Analytic Characterization of Shear Localization in Thermoviscoplastic Materials," J. Appl. Mechs., **54**, 806.

1987 WRIGHT, T.W., and WALTER, J.W., "On Stress Collapse in Adiabatic Shear Bands," J. Mech. Phys. Solids, **35**, 701.

1988 ANAND, L., LUSH, A.M., and KIM, K.H., "Thermal Aspects of Shear Localization in Viscoplastic Solids," Thermal Aspects in Manufacturing, In ATTIA, M.H. and KOPS, L. (eds.), ASME-PED-Vol. 30, 89–103.

1988 MARCHAND, A., and DUFFY, J., "An Experimental Study of the Formation Process of Adiabatic Shear Bands in a Structural Steel," J. Mechs. Phys. Solids, **36**, 251.

1989 BATRA, R.C., "Effect of Inertial Forces on the Initiation and Growth of Shear Bands in Viscoplastic Materials," Proc. 26th Annual Meeting of the Society of Engineering Science, Ann Arbor, September 1989, p. 176. (Also see Applied Mechs. Revs., **45**, 5123, 1992.)

1989 BATRA, R.C., and LIU, D.S., "Adiabatic Shear Banding in Dynamic Plane Strain Problems," J. Appl. Mechs., **56**, 527.

1989 NEEDLEMAN, A., "Dynamic Shear Band Development in Plane Strain," J. Appl. Mechs., **56**, 1.

1989 SHAWKI, T., and CLIFTON, R.J., "Shear Band Formation in Thermal Viscoplastic Materials," Mechs. Materials, **8**, 13.

1990 BATRA, R.C., and KIM, C.H., "Adiabatic Shear Banding in Elastic-Viscoplastic Nonpolar and Dipolar Materials," Int. J. Plasticity, **6**, 127.

1990 BATRA, R.C., and LIU, D.S., "Adiabatic Shear Banding in Dynamic Plane Strain Compression of a Viscoplastic Material," Int. J. Plasticity, **6**, 231.

1990 WRIGHT, T.W., "Approximate Analysis for the Formation of Adiabatic Shear Bands," J. Mech. Phys. Solids, **38**, 515.

1990 ZHU, Z.G., and BATRA, R.C., "Dynamic Shear Band Development in Plane Strain Compression of a Viscoplastic Body Containing a Rigid Inclusion," Acta Mechanica, **84**, 89.

Department of Mechanical and Aerospace Engineering and Engineering Mechanics
University of Missouri–Rolla
Rolla, MO 65401-0249, USA

(*Received* 24 *March* 1990; *in final revised form* 15 *March* 1991)